

Reliability Assessment on Deep Braced Excavations Adjacent to High Slopes in Mountain Cities

RH. Zhang¹ WG.zhang^{1,2} ZJ.Hou¹ and W.Wang¹

¹School of Civil Engineering, Chongqing University, Chongqing, China

²Key Laboratory of New Technology for Construction of Cities in Mountain Area, Chongqing University, Chongqing, China.
E-mail: cheungwg@126.com

ABSTRACT: Due to rapid urbanization, the land available for construction becomes more and more scarce. Within a built-up environment, the construction safety of a deep excavation becomes more crucial with the ever-increasing building density. For deep excavations in mountain cities, the areas of the foundation pit to be excavated are generally the passive soil pressure zones for the upper existing slope. Construction disturbance, weakening of the passive area, as well as the formation of even higher slope through superposition of foundation pit to the upper slope, will result in more deformation and even failure of the slope. This study numerically investigates the influences of excavation geometries, the system stiffness and the distance between the excavation and slope and develops simplified ultimate and serviceability limit state models with regard to the overall factor of safety and the maximum lateral wall deflection of the supporting system, respectively. Considering the uncertainties of the design parameters, a probabilistic framework combining the estimation models with First-Order Reliability Method (FORM) is proposed to determine the probability that a threshold factor of safety or the maximum wall deflection is exceeded. The study presents preliminary guidelines for reliability assessment of ultimate and serviceability limit state designs for deep braced excavations adjacent to high slopes in mountain cities.

Keywords: braced excavation, upper slope, wall deflection, factor of safety, reliability assessment.

1. INTRODUCTION

With promotion of the Belt and Road Initiatives in China, the fast development of urbanization progress has brought the great demand of commodity housing and public transport facilities. Thus it is inevitable that more deep excavations to be constructed for residence, commercial buildings as well as the sky scrapers designed aside the existing slopes in densely populated mountainous cities such as Chongqing and Guiyang. It is well known that for deep excavations in mountain cities, the areas of the foundation pit to be excavated are generally also the passive soil pressure zones for the upper existing slopes. Consequently, the construction disturbances, weakening of the passive area, as well as the formation of the even higher slope through superposition of foundation pit to the upper slope, will result in more deformation and even collapse of the slope. Nevertheless, there are few investigations of the interaction between braced excavation and the adjacent slope and the influence of such interaction on the overall stability. Li et al. (2011) investigated the stability of supporting system and the safety of deep braced excavation adjacent to slope, through analyzing the influence of excavation of Shangshuijing station Shenzhen Metro Line 5 on side slope using FLAC3D. Wang et al. (2011) examined the deformation characteristics and behaviors of retaining structures for a complex geotechnical system comprising of a high building slope and a nearby deep excavation, based on field instrumentations. Varzaghani and Ghanbari (2014) presented a new analytical model to determine the seismic displacements of the shallow foundations adjacent to slopes. However, there is still a lack of systematic investigation of the key influential factors and the effects on the ultimate limit state and serviceability limit state of the excavation and slope system.

In this study, the global factor of safety FS obtained via the shear strength reduction (SSR) technique (also called c/ϕ reduction method) is used as the criterion for the ultimate limit state and the calculated maximum lateral wall deflection is adopted as the serviceability limit state criterion. It then numerically investigates the influences of the excavation geometries, the supporting system stiffness, the distance between the new excavation and the existing slope on excavation responses including the global FS and the wall deflection using PLAXIS software. Estimation models with regard to both the ultimate and serviceability limit states are developed. Probabilistic framework combining the proposed estimation models with the First-Order Reliability Method (FORM) is adopted to determine the probability that a threshold factor of safety or the maximum wall deflection is exceeded. This proposed approach enables a cost-effective analysis to be conducted for a rational design of excavation system adjacent to an existing high slope.

2. FINITE ELEMENT ANALYSIS

2.1 Numerical modeling

The PLAXIS^{2D} software was utilized for the numerical simulations. The Mohr-Coulomb constitutive model was selected for the soil. A typical cross-section of the excavation and slope system, the geometries as well as the properties of the soil and the supporting elements are shown in Figure 1.

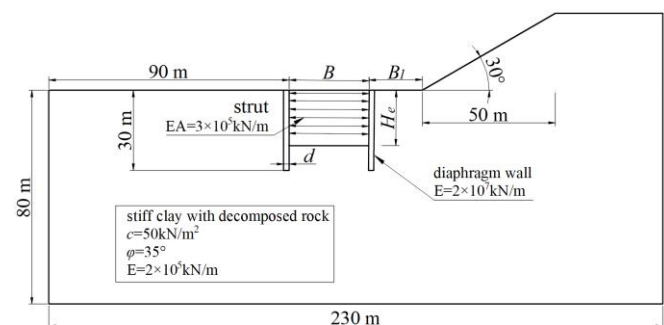


Figure 1 Cross-sectional soil and wall profile

The analyses considered a plane strain excavation supported by a retaining wall system near an unreinforced slope. The soil was modeled by 15-noded triangular elements. The structural elements were assumed to be linear elastic with the wall represented by 5-noded beam elements and 3-noded bar elements were used for the 6 levels of struts located at depths of 1 m, 4 m, 7 m, 10 m, 13 m and 16 m below the original ground surface. The nodes along the side boundaries of the mesh were constrained from displacing horizontally while the nodes along the bottom boundary were constrained from moving horizontally and vertically. The left and right vertical boundary extend far from the excavation to minimize the effects of the boundary restraints. The ranges of the design parameters varied are shown in Table 1.

The strut stiffness per meter EA is assumed as a constant at $3.0 \times 10^5 \text{ kN/m}$ since the influence of strut stiffness on wall deflection is not very significant when the strut is stiff (Poh and Wong 1997). A total of 162 hypothetical cases were analysed.

The construction sequence comprised the following steps:

- the wall is installed ("wished into place") without any disturbance in the surrounding soil;

- the soil is excavated uniformly 1 m below each target strut level prior to adding the strut support with struts at 3 m vertical spacing until the final depth H_e is reached.
- Each phase of strut installation is followed by a subsequent phase of global safety factor calculations by SSR method.

Details are listed in Table 2.

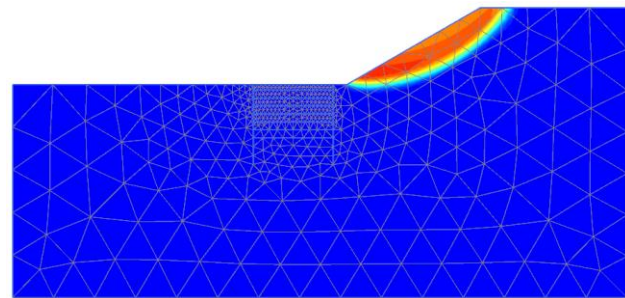
Table 1 Parameters considered and the ranges

Parameters	Ranges
*System stiffness S	3.794, 4.605, 5.187
Excavation width B (m)	20, 30, 40
Excavation depth H_e (m)	14, 17, 20
Wall thickness d (m)	0.6, 0.9, 1.2
distance between braced excavation and side slope B_1 (m)	5, 10, 15, 20, 30, 40
Penetration ratio D/H_e	0.50, 0.76, 1.14

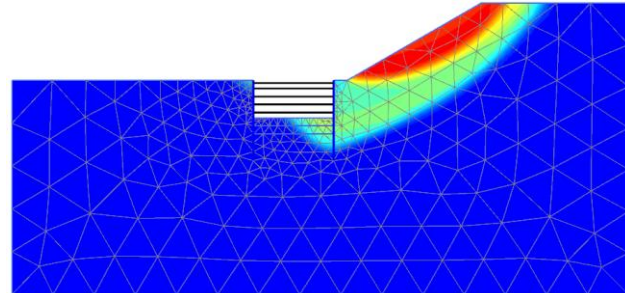
* Influence of wall stiffness was studied by varying wall thickness d while keeping the Young's modulus of the wall constant ($E=1.20 \times 10^6$ kN/m²). The corresponding natural logarithm of the system stiffness $\ln(EI/\gamma_w h^4_{avg})$, denoted by S for the wall thickness of 0.6, 0.9 and 1.2 m with average vertical strut spacing $h_{avg}=3$ m

Table 2 Construction procedures

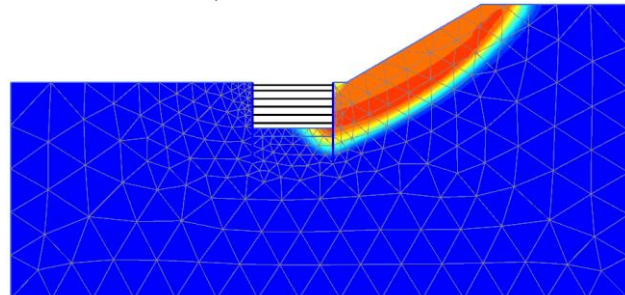
Phases	Construction details
Initial Phase	Generate the initial effective stress, pore pressure and state parameters.
Phase 1	Calculated the global safety factor by SSR method
Phase 2	Install the diaphragm wall
Phase 3	Reset displacement to zero, excavate to 2 m below the ground surface inside the excavation, install strut at 1 m below the ground surface
Phase 4	Excavate to 5 m below the ground surface
Phase 5	Install strut at 4 m below the ground surface
Phase 6	Calculated the global safety factor by SSR method
Phase 7	Excavate to 8 m below the ground surface
Phase 8	Install strut at 7 m below the ground surface
Phase 9	Calculated the global safety factor by SSR method
Phase 10	Excavate to 11 m below the ground surface
Phase 11	Install strut at 10 m below the ground surface
Phase 12	Calculated the global safety factor by SSR method
Phase 13	Excavate to 14 m below the ground surface
Phase 14	Install strut at 13 m below the ground surface
Phase 15	Calculated the global safety factor by SSR method
Phase 16	Excavate to 17 m below the ground surface
Phase 17	Install strut at 16 m below the ground surface
Phase 18	Calculated the global safety factor by SSR method
Phase 19	Excavate to 20 m below the ground surface
Phase 20	Calculated the global safety factor by SSR method



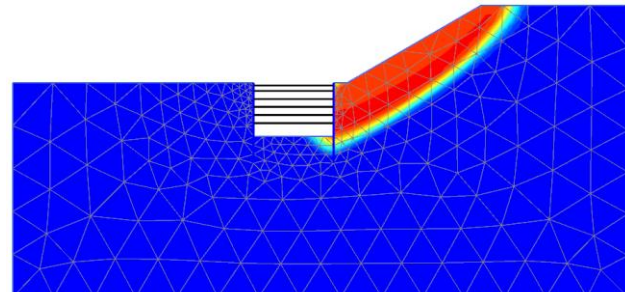
a) $H_e=0$ m $FS=2.341$



b) $H_e=14$ m $FS=2.214$



c) $H_e=17$ m $FS=2.095$



d) $H_e=20$ m $FS=1.705$

Figure 2 Contour of slip surface and FS for different excavation depths H_e for $B=30$ m, $B_1=5$ m, $S=4.605$

2.2 Numerical results

The numerical results include the factor of safety FS and the maximum lateral wall deflection δ_{hm} . FS is solved through SSR technique, in which the shear strengths are systematically reduced until failure occurs. This procedure was proposed by Zienkiewicz et al. (1975), and improved by Brinkgreve and Bakker (1991). It has been verified by Lian et al. (2001) that the SSR FE method can be widely applied in the engineering practice since this method takes advantages over the conventional limit equilibrium method. Cheng et al. (2007) and Dawson et al. (1999) proved that the SSR technique perform well in many slope cases.

Figure 2 plots the variation of slip surface contours as excavation proceed, for case of $B=30$ m, $B_1=5$ m, $S=4.605$. The FS values for excavation depths H_e of 0, 14, 17, 21 m are also calculated, respectively. It can be observed that as excavation proceeds, FS values decrease. The smallest FS is about 1.705 with a decrease of 0.636 from the original 2.341. In addition, it is also clear that a larger slip surface occurred when the excavation depth H_e becomes greater.

Figure 3 presents some typical plots of the FS decrease for different B_1 for $H_e=20$ m, $S=4.605$. Generally, the FS decrease becomes less significant as the distance between the excavation and the existing slope B_1 increases and converges to 0, indicating that the further away the excavation is from the existing slope, the much safer the whole system is. In addition, for the model dimensions considered in this study, the braced excavation has no impact on stability of the adjacent slope when the separation B_1 is greater than 40 m. As for the lateral deflections of the retaining wall on the slope side, Figure 4 shows the maximum lateral wall deflection δ_{hm} for different distances B_1 for case of $H_e=20$ m, $S=4.605$. It is clear that δ_{hm} has a tendency to grow with excavation width B while it decreases with the increase of the separation B_1 .

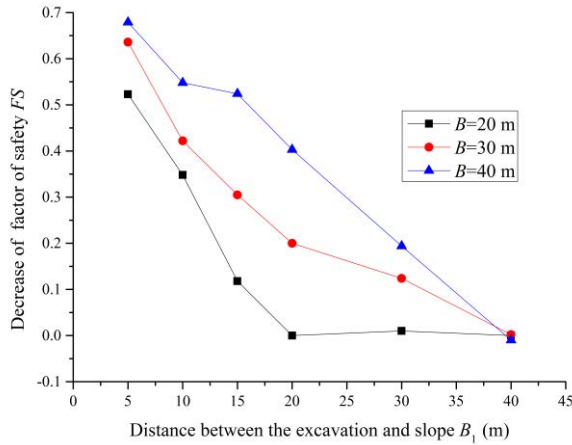


Figure 3 Decrease of factor of safety FS on different B1 for He=20 m, S=4.605

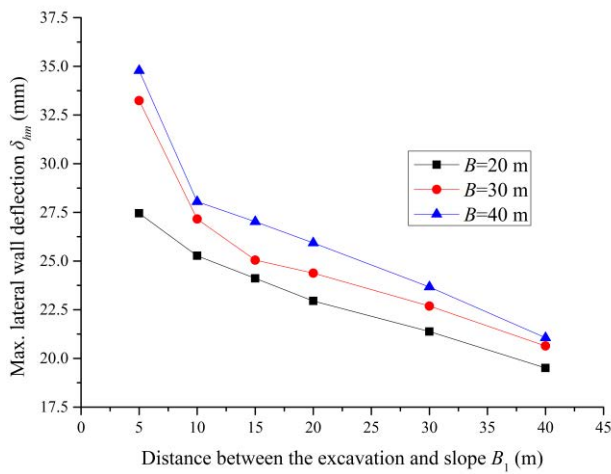


Figure 4 Max. lateral wall deflection δ_{hm} for different B1 of case He=20 m, S=4.605

3 ESTIMATION MODELS FOR THE LIMIT STATE FUNCTIONS

For the performance in deep braced excavations, especially for the excavations adjacent to high slopes, both the ultimate limit state (ULS) and the serviceability limit state (SLS) should be satisfied. In the following sub sections, the limit state functions for ULS and SLS are developed respectively, based on the numerical results in the previous section.

3.1 Ultimate limit state model

Based on the calculated FS results, a Polynomial Regression (PR) model has been developed for estimating the factor of safety FS as a function of four input parameters: B, B₁, H_e and S in Eq. (1), with a coefficient of determination R² of 0.881, as below

$$FS = 7.35 \times 10^{-2} B - 1.57 \times 10^{-1} B_1 + 3.51 \times 10^{-2} H_e + 1.02 S - 2.5 \times 10^{-6} B^2 - 2.29 \times 10^{-4} B_1^2 - 8.07 \times 10^{-4} H_e^2 - 2.22 \times 10^{-2} S^2 + 2.4 \times 10^{-4} B B_1 - 4.08 \times 10^{-3} B H_e + 1.65 \times 10^{-4} B S + 8.01 \times 10^{-3} H_e B_1 - 1.56 \times 10^{-3} S B_1 - 2.8 \times 10^{-2} H_e S - 1.84 \times 10^{-2} B (D/H_e) + 4.83 \times 10^{-2} B_1 (D/H_e) + 9.4 \times 10^{-2} H_e (D/H_e) - 3.55 \times 10^{-1} S (D/H_e) \quad (1)$$

Figure 5 plots the estimated factor of safety FS_{FEM} values against the calculated FS_{EST} results. Also shown are the 100% agreement line and the 10% error lines, indicating that Eq. (1) is fairly accurate in predicting the global factor of safety for deep braced excavations adjacent to high slopes since the majority of data points are within the error lines.

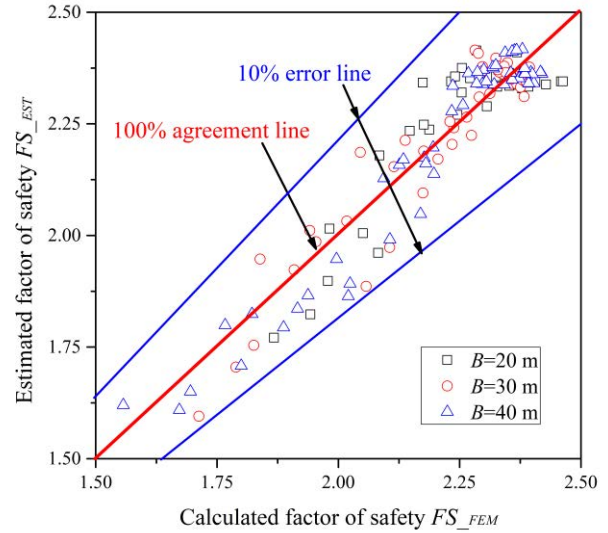


Figure 5 Comparison between FS_{FEM} and FS_{EST}

3.2 Serviceability limit state model

Similarly, a Logarithmic Regression (LR) model for predicting the maximum lateral wall deflection δ_{hm} is developed and shown in Eq. (2), with fairly high coefficient of determination R²=0.946, as below

$$\delta_{hm} = 0.1133 B^{0.1086} B_1^{-0.223} (H_e)^{2.1247} (D/H_e)^{0.0568} S^{-0.4448} \quad (2)$$

Figure 6 plots the estimated maximum lateral wall deflections δ_{hm_EST} values against the calculated results δ_{hm_FEM} . Also shown are the 100% agreement line and the 20% error lines, indicating that Eq. (2) is fairly accurate in predicting the maximum wall deflections induced by deep braced excavations adjacent to high slopes.

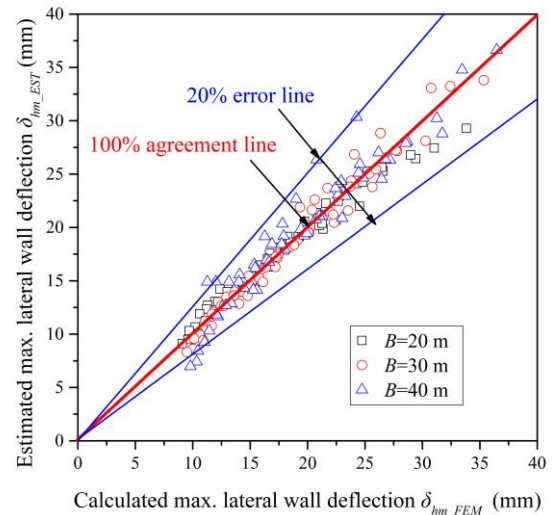


Figure 6 Comparison between δ_{hm_FEM} and δ_{hm_EST}

4. PROBABILISTIC ASSESSMENT OF THE LIMIT-STATES

In many civil engineering applications, the assessment of safety is made by firstly establishing a relationship between the load S of the system and the resistance R. The boundary separating the safe and 'failure' domains is the limit state surface (boundary) defined by $G(x) = R - S = 0$, where x is vector of the random variables. Mathematically, $R > S$ or $G(x) > 0$ would denote a 'safe' domain. An unsatisfactory or 'failure' domain occurs when $R < S$ or $G(x) < 0$. Calculation of Pf involves the determination of the joint probability distribution of R and S and the integration of the Probability Density

Function (PDF) over the failure domain. Considering that the PDFs of the random variables are not known in most geotechnical applications and the integration is computationally demanding when multi-variables are involved, an approximate method, known as the First-Order Reliability Method (FORM) (Hasofer and Lind, 1974), is commonly used to assess the probability failure P_f . (Low 1996) has shown that Microsoft EXCEL spreadsheet can be used to perform the minimization and determine reliability index β .

The reliability index β and the probability of failure P_f for both the ultimate and the serviceability limit states can be performed using FORM based on the built PR and LR models. The ULS model Eq. (1) is incorporated into an EXCEL spreadsheet environment based on the approach by (Low and Tang 2007), from which the reliability index β can be determined. Figure 7 shows a sample spreadsheet for computing the factor of safety FS where the statistics of the design parameters are the same as those used in the previous section. The spreadsheet cells B3:B5 allows the selection of various distribution types for the input variables, including normal, lognormal, triangular etc. as explained in (Low and Tang

2007). For nonnormals, the nonnormal distributions are replaced by an equivalent normal ellipsoid, centred at the equivalent normal mean. Cells D3:E5 are parameters which are set corresponding to the normal distribution in this study. The correlation matrix R in cells G3:I5 are used to define the correlations between B , H_e and S . The n_i vector in cells J3:J5 contains equations for $(x_i - u_i^N) / \sigma_i^N$. The design point (x^* values) was obtained by using the spreadsheet's built-in optimization routine SOLVER to minimize the cell, by changing the x^* values, under the constraint that the performance function $G(x^*) = 0$. Prior to invoking the SOLVER search algorithm, the x^* values were set equal to the mean values (30, 17, 4.5) of the original random variables. Iterative numerical derivatives and directional search for the design point x^* were automatically carried out in the spreadsheet environment.

Probabilistic assessment of SLS in Figure 8 is almost the same as Figure 7 except the $G(x)$ formulations. For the detailed procedures in performing the FORM spreadsheet framework to derive β and the corresponding P_f , the paper published by Zhang and Goh (2012) can be referred to.

	A	B	C	D	E	F	G	H	I	J	K	L	M	N	O	P	Q	R
1																		
2																		
3																		
4																		
5																		
7																		
8																		

mathematical equation for ULS using $G(x)=FS-FS_{cr}$
 $=7.35 \times 10^{-2}B - 1.57 \times 10^{-1}B_1 + 3.51 \times 10^{-2}H_e + 1.02S - 2.5 \times 10^{-6}B^2 - 2.29 \times 10^{-4}B_1^2$
 $- 8.07 \times 10^{-4}H_e^2 - 2.22 \times 10^{-2}S^2 + 2.4 \times 10^{-4}BB_1 - 4.08 \times 10^{-3}BH_e + 1.65 \times 10^{-4}BS$
 $+ 8.01 \times 10^{-3}H_eB_1 - 1.56 \times 10^{-3}SB_1 - 2.8 \times 10^{-2}H_eS - 1.84 \times 10^{-2}B(D/H_e) + 4.83 \times 10^{-2}B_1(D/H_e)$
 $+ 9.4 \times 10^{-2}H_e(D/H_e) - 3.55 \times 10^{-1}S(D/H_e) - FS_{cr}$

Probabilistic parameters

design point

Distribution	Random variables	Average	S.D.	x_i^*	Correlation matrix [R]	n_i	$G(\underline{x})$	β	$P_f(\%)$
Normal	B (m)	30	3	30.07	1 0 0	0.02405	1.661	2.3330	0.9824
Normal	H_e (m)	17	0.51	17.07	0 1 0	0.14089			
Normal	S	4.5	0.45	4.279	0 0 1	-0.49155			
Deterministic	B_1	10							
	D/H_e	1							

$P_f \approx 1 - \Phi(\beta)$

$\beta = \text{SQRT}(\text{MMULT}(\text{TRANSPOSE}(J3:J5), \text{MMULT}(\text{MINVERSE}(\text{crmat}), J3:J5)))$
 invoke solver to minimise β by changing n_i values subject to $G(x)=0$

Figure 7 Calculation on β and P_f for ultimate limit state using FORM spreadsheet

	A	B	C	D	E	F	G	H	I	J	K	L	M	N	O	P	Q
1																	
2																	
3																	
4																	
5																	
7																	
8																	

mathematical equation for SLS using $G(x)=\delta_{lim,cr}-\delta_{lim}$
 $=\delta_{lim,cr}-0.1133B^{0.1086}B_1^{-0.223}(H_e)^{2.1247}(D/H_e)^{0.0568}S^{0.4448}$

Probabilistic parameters

design point

Distribution	Random variables	Average	S.D.	x_i^*	Correlation matrix [R]	n_i	$G(\underline{x})$	β	$P_f(\%)$
Normal	B (m)	30	3	30.07	1 0 0	0.02405	0.000	5.6840	0.0000
Normal	H_e (m)	17	0.51	17.07	0 1 0	0.14089			
Normal	S	4.5	1.8	3.615	0 0 1	-0.49155			
Deterministic	B_1	10							
	D/H_e	1							

$P_f \approx 1 - \Phi(\beta)$

$\beta = \text{SQRT}(\text{MMULT}(\text{TRANSPOSE}(J3:J5), \text{MMULT}(\text{MINVERSE}(\text{crmat}), J3:J5)))$
 invoke solver to minimise β by changing n_i values subject to $G(x)=0$

Figure 8 Calculation on β and P_f for serviceability limit state using FORM spreadsheet

4.1 Probabilistic assessment of the ultimate limit state

For either the braced excavation or the slope, there are design guidance with regard to the choice of the critical factor of safety. However, for the excavation and slope system, there are no guidelines for the determination of such critical safety factor values. Thus the influence of the critical factor of safety FS_{cr} on β and P_f of ULS is examined in this study.

Figure 9 plots the influence of the various design parameters on the β and P_f of ULS. It is clear that both the coefficient of variation of the system stiffness $COVS$ and the critical factor of safety FS_{cr} significantly influence the β and P_f . In addition, the influence of $COVS$ on β and P_f is also as significant as that for FS_{cr} . The plots in Figure 10 indicate that the influence of either B_1 or $COVS$ on β and P_f is also obvious when different excavation widths B of 20, 30, 40 m are considered.

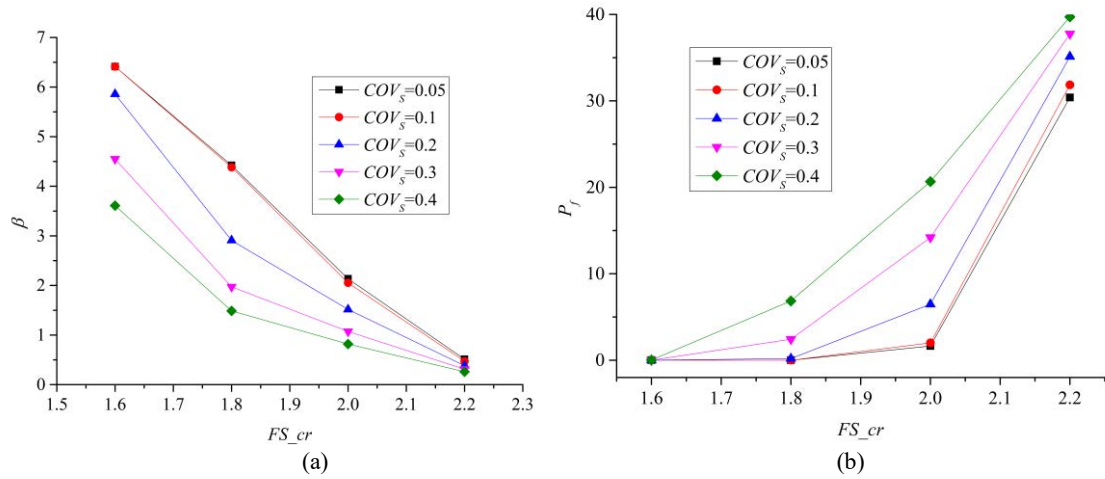


Figure 9 Influence of COVS and FS_cr on (a) β and (b) P_f for $B_1=5\text{m}$, $B=30\text{m}$, $H_e=17\text{m}$, $S=4.5$

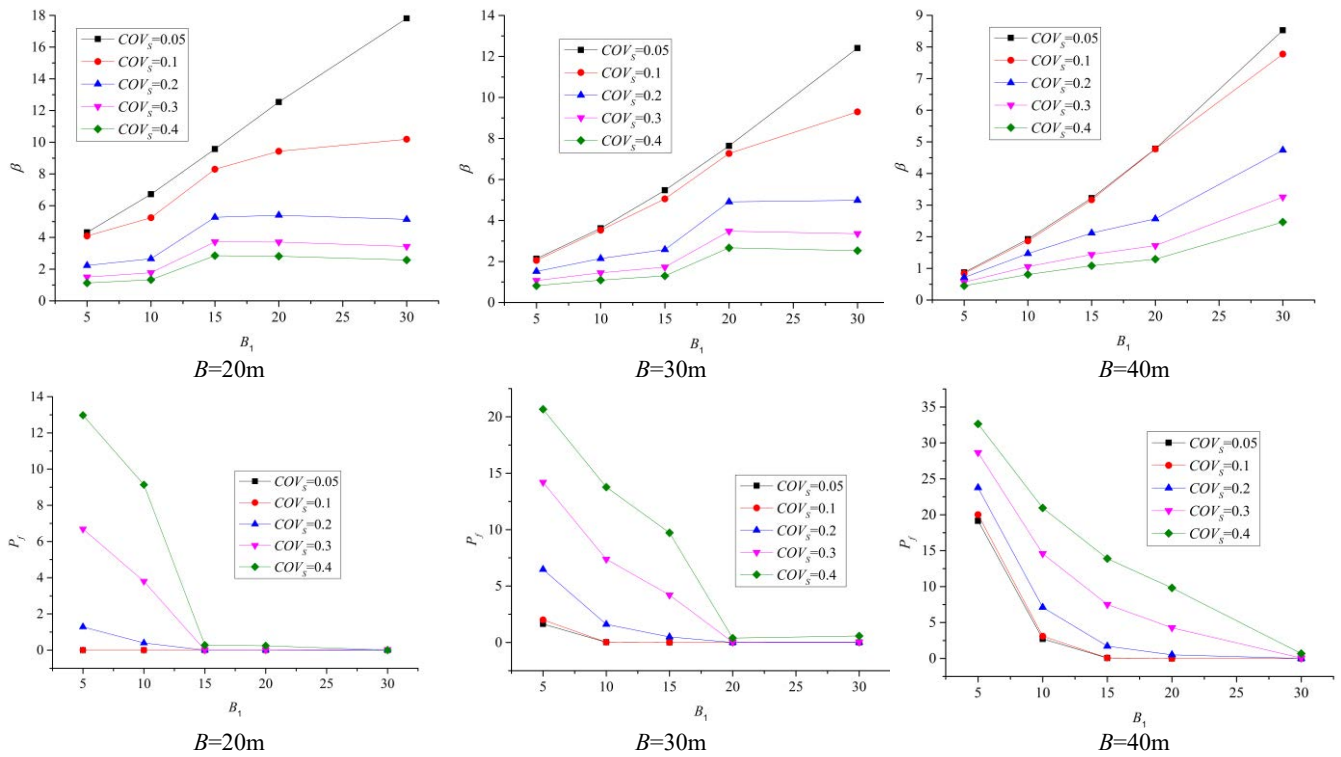


Figure 10 Influence of COVS and B_1 on β and P_f for $B=20, 30, 40\text{ m}$, $H_e=17\text{m}$, $S=4.5$, $FS_{cr}=2.0$

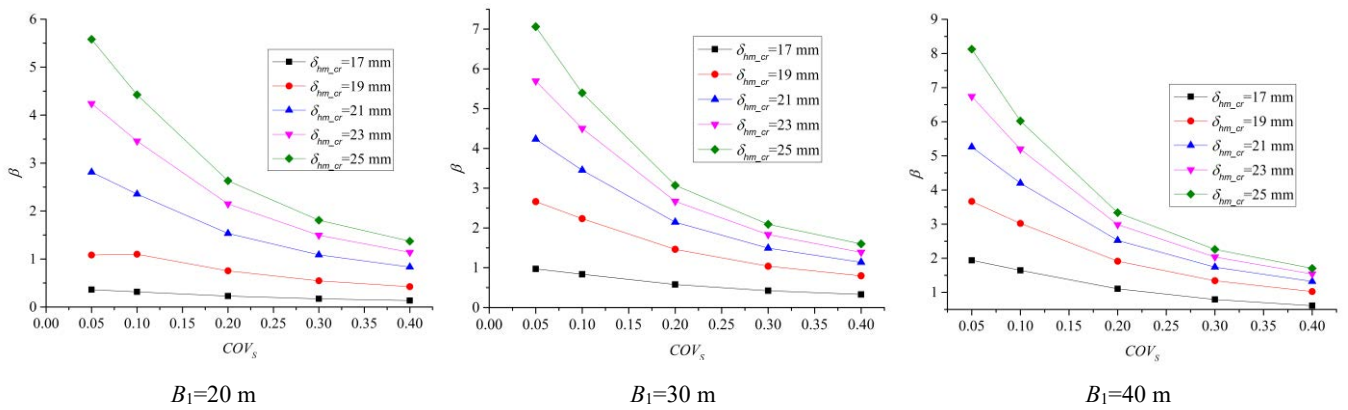


Figure 11 Influence of $COVS$ and δ_{hm_cr} on β for $B=30\text{ m}$, $H_e=17\text{m}$, $S=4.5$, $B_1=20, 20, 40\text{ m}$

Figure 10 also compares the influence of both the COV_S and B_1 on β and P_f for $B=20, 30, 40$ m, respectively, for $H_e=17$ m, $S=4.5$, and chosen critical factor of safety $FS_{cr}=2.0$. It is obvious that β becomes greater with increase of the excavation width B_1 while decreases with the increase of excavation width B . Meanwhile, P_f decreases as the excavation becomes further away from the slope. A greater excavation width B generally results in a larger P_f . Generally P_f converges to 0 when the separation is sufficient. However, different B causes different convergence speeds.

4.2 Probabilistic assessment of the serviceability limit state

There are also discussions as for the choice of the threshold lateral wall deflections for serviceability considerations. Figure 11 plots the influence of COV_S and the critical max. wall deflection δ_{hm_cr} on β and P_f for $B=30$ m, $H_e=17$ m, $S=4.5$ and $B_1=20, 20, 40$ m, respectively, indicating that both COV_S and δ_{hm_cr} significantly influence the β and P_f . However, the influence of COV_S on β and P_f is not as significant as that for δ_{hm_cr} , especially when COV_S is greater than 0.20. β has a tendency to grow with the critical maximum lateral wall deflections δ_{hm_cr} since the probability that a greater threshold is exceeded is much lower. β decreases with the increase of COV_S . In addition, it can be observed that the influence of B_1 on β is also significant since β increases substantially with the separation B_1 .

Figure 12 shows the influence of COV_S on β for $H_e=17$ m, $S=4.5$, $\delta_{hm_cr}=23$ mm, $B=20, 30, 40$ m and $B_1=10, 15$ m respectively. It is clear that β decreases as the variation of the system stiffness becomes greater. It is logical that β increases when the excavation is becoming further away from the slope.

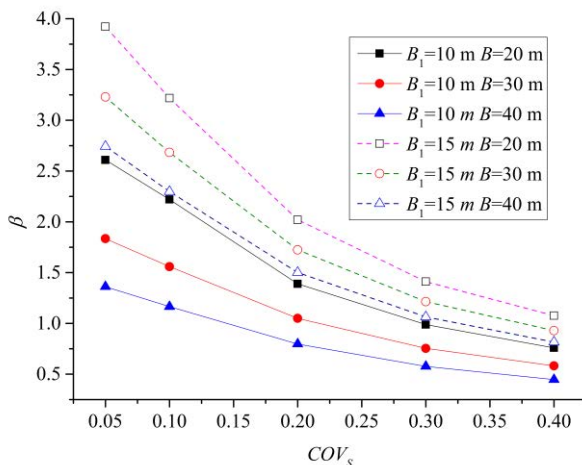


Figure 12 Influence of COV_S on β for $H_e=17$ m, $S=4.5$, $\delta_{hm_cr}=23$ mm, $B=20, 30, 40$ m and $B_1=10, 15$ m

5. SUMMARY AND CONCLUSIONS

This paper presents numerical investigations about influence of braced excavation on the existing slope, from perspectives of the global factor of safety and the maximum lateral wall deflections. It also proposed probabilistic framework for quantitative assessment of both the ultimate and the serviceability limit states in view of some design and construction uncertainties.

Regression models for the ultimate and serviceability limit states are developed respectively. Through the use of the automated spreadsheet search algorithm to determine the design point, to meet the different target performance levels, the critical FS or the threshold max. lateral wall deflection can be obtained. The influences of the key parameters, as well as the design uncertainties on the reliability index and the probability failure are examined. The procedures outlined in this paper can be used to obtain a rational design of braced excavation adjacent to high slope and a cost-effective analysis.

6. REFERENCES

- Brinkgreve, R.B.J., Bakker, H.L.(1991). "Non-linear finite element analysis of safety factors." In: Proc. 7th Int. Conf. on Computer Methods and Advances in Geomechanics, vol. 23, pp. 1117-1122.
- Cheng, Y. M., et al. (2007). "Two-dimensional slope stability analysis by limit equilibrium and strength reduction methods." Computers and Geotechnics 34(3): pp 137-150.
- Dawson, E. M., et al. (1999). "Slope stability analysis by strength reduction." Geotechnique 49(6): pp 835-840.
- Hasofer, A.M., Lind, N.(1974). "An exact and invariant first-order reliability format." J. Eng. Mech. ASCE 100 (1), pp 111-121.
- Li, Y. H., et al. (2011). "Stability and Safety Analysis of Braced Excavation for Subway Station during Construction under the Condition of Side Slope." Applied Mechanics and Materials 99-100: pp 1166-1170.
- Lian, Z.-y., et al. (2001). "Stability analysis of excavation by strength reduction FEM." Chinese Journal of Geotechnical Engineering 23(4):p 5.
- Low, B.K.(1996). "Practical probabilistic approach using spreadsheet." In: Shackelford, C.D., Nelson, P.P., Roth, M.J.S. (Eds.), Uncertainty in the Geologic Environment, GSP 58. ASCE, Reston, pp. 1284-1302.
- Low, B.K. and Tang, W.H. (2004), "Reliability analysis using object-oriented constrained optimization." Struct. Saf., 26(1), pp 69-89.
- Low, B.K. and Tang, W.H. (2007), "Efficient spreadsheet algorithm for first-order reliability method." J.Eng. Mech. ASCE, 133(12), pp 1378-1387.
- Poh TY, Wong IH, Chandrasekaran B, (1997) "Performance of two propped diaphragm walls in stiff residual soils." Journal of Performance of Constructed Facilities, 11(4): pp 190-199.
- Varzaghani, M. I., & Ghanbari, A. (2014). "A new analytical model to determine dynamic displacement of foundations adjacent to slope." Geomechanics and Engineering. pp 561-575.
- Wang, Q., et al. (2011). "analysis of slip-risk and dynamic monitoring of a high building slope fringed a deep foundation pit." journal of safety and environment .11(2):p 6.(in Chinese)
- Zhang, W. and A. T. C. Goh (2012). "Reliability assessment on ultimate and serviceability limit states and determination of critical factor of safety for underground rock caverns." Tunnelling and Underground Space Technology 32: pp 221-230.
- Zienkiewicz, O.C., et al.(1975). "Associated and non-associated visco-plasticity in soil mechanics." Geotechnique 25 (4), pp 671-689.